Enhanced interaction effects in the vicinity of the topological transition

C. C. A. Houghton, E. G. Mishchenko, and M. E. Raikh
Department of Physics and Astronomy, University of Utah, Salt Lake City, Utah 84112, USA

(Received 15 August 2019; published 25 October 2019)

A metal near the topological transition can be loosely viewed as consisting of two groups of electrons. The first group are "bulk" electrons occupying most of the Brillouin zone. The second group are electrons with wave vectors close to the topological transition point. Kinetic energy, $\tilde{E}_F$, of electrons of the first group is much bigger than kinetic energy, E_F, of electrons of the second group. With electrons of the second group being slow, the interaction effects are more pronounced for these electrons. We perform a calculation illustrating that electrons of the second group are responsible for inelastic lifetime making it anomalously short, so the concept of quasiparticles applies to these electrons only marginally. We also demonstrate that interactions renormalize the spectrum of electrons in the vicinity of topological transition, the parameters of renormalized spectrum being strongly dependent on the proximity to the transition. Another many-body effect that evolves dramatically as the Fermi level is swept through the transition is the Friedel oscillations of the electron density created by electrons of the second group around an impurity. These oscillations are strongly anisotropic with a period depending on the direction. Scattering of electrons off these oscillations give rise to a temperature-dependent ballistic correction to the conductivity.

DOI: 10.1103/PhysRevB.100.165140

I. INTRODUCTION

Topological transitions in metals take place when, upon changing a certain external parameter, the connectivity of the Fermi surface undergoes a transformation. The concept of topological transitions was introduced by I. M. Lifshitz in 1960 [1]. Lifshitz demonstrated that thermodynamic characteristics of a metal exhibit a singular behavior in the vicinity of the transition. Such a singular behavior was subsequently observed experimentally [2,3]. First, experiments were conducted on 3D metallic alloys [2] and 2D semiconductor superlattices [3]. In the past decade, the class of materials in which the signatures of the topological transitions were uncovered has significantly broadened [4–11] to include heavy fermions, graphite, germanene, cilicene, ruthinades, etc.

On the theoretical side, kinetic and thermodynamic characteristics of metals near the topological transitions [12–18] were actively studied after the experiments [2,3]. The results are reviewed in Ref. [19]. On the conceptual level, the main theoretical finding is that, in addition to the single-particle density of states, the transition manifests itself in the energy dependence of the impurity scattering time of carriers, which, at the same time, broadens the transition. Recent theoretical interest in the topological transitions [20–25] is mostly motivated by the invention of materials with strong spin-orbit coupling.

The role played by electron-electron interactions in the topological transition was considered in Ref. [18] with a general conclusion that, away from Pomeranchuk instability, Fermi-liquid effects renormalize the singular part of thermodynamic quantities.

The goal of the present paper is to trace how the standard many-body effects for an isotropic spectrum get modified in the vicinity of the topological transition. We will consider the following effects: Friedel oscillations of the electron density, interaction-induced modification of the electron spectrum, and the interaction-induced electron lifetime caused by the creation of the electron-hole pairs. We find that the proximity to the transition gives rise to additional Friedel oscillations with very long periods, which are strongly anisotropic and get rotated by 90° as the Fermi level is swept through the transition.

Our main finding is that the electron lifetime, τ_e, associated with the creation of pairs, shortens dramatically in the vicinity of the transition. Directly at the transition, we have $\frac{\hbar}{\tau_e(E)} \sim E$, so the concept of the Fermi liquid applies only marginally.

Since the interaction effects are more pronounced in two dimensions, we will choose the simplest form of the spectrum in the vicinity of the topological transition

$$E_{\mathbf{k}} = \frac{\hbar^2 k_x^2}{2m} - \frac{\hbar^2 k_y^2}{2m}, \tag{1}$$

see Fig. 1. The transition corresponds to the position of the Fermi level $E_F = 0$. As E_F changes from negative to positive, the Fermi surface near $k_x = k_y = 0$ evolves as illustrated in Fig. 2. Most importantly, the typical wave vector, $(\frac{mE_F}{\hbar^2})^{1/2}$, in the vicinity of the transition is small, while everywhere else in the Brillouin zone this wave vector is big, namely it is of the order of $(\frac{m\tilde{E}_F}{\hbar^2})^{1/2}$, where $\tilde{E}_F$ is the Fermi level measured from the bottom of the band.

While within a single-particle approach the topological transition causes a singular correction to the electron characteristics, interaction effects give rise to new *distinct* features, in particular, new Friedel oscillations and a new channel of inelastic relaxation.

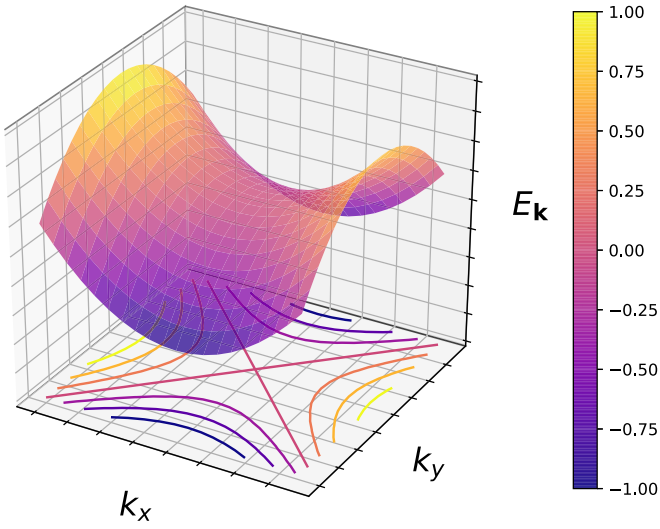

FIG. 1. Electron spectrum near the topological transition is plotted from Eq. (1) together with Fermi contours for different values of the Fermi energy, E_F.

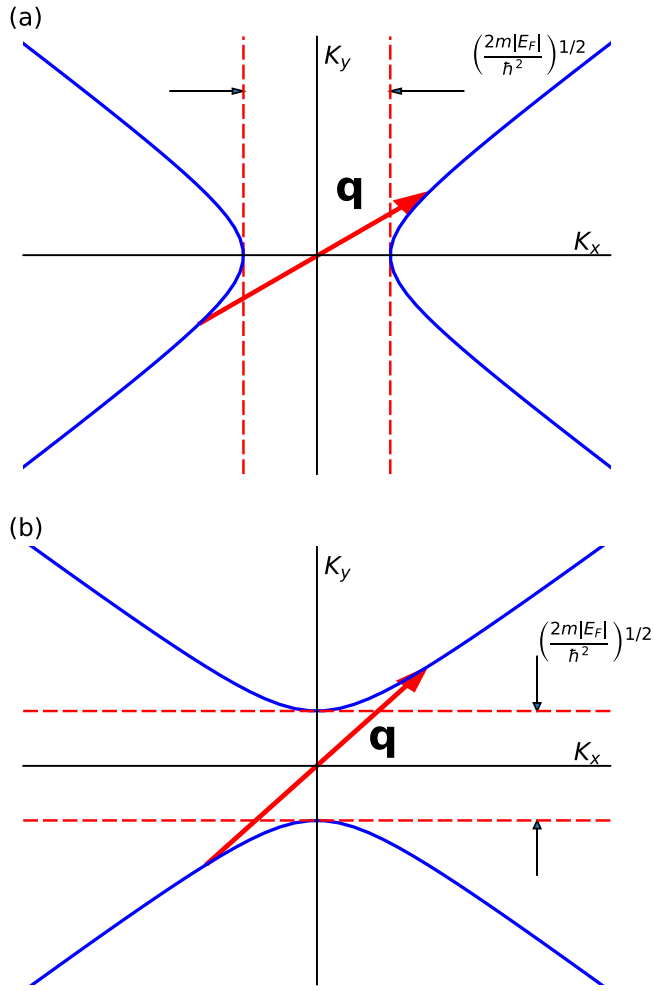

FIG. 2. The process responsible for the formation of the Kohn anomaly and ensuing long-period Friedel oscillations is illustrated for positive E_F (a) and negative E_F (b). The components of the vector $\mathbf{q}$ satisfy the condition $q_x^2 - q_y^2 = 4k_F^2$, Eq. (39).

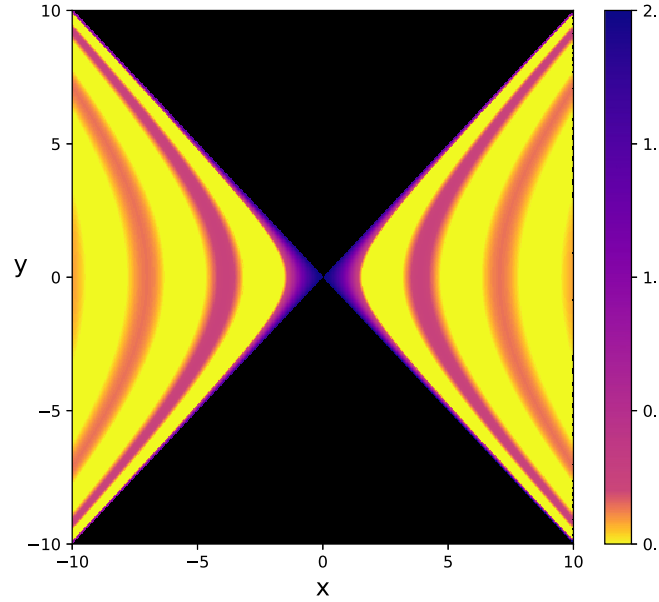

FIG. 3. Anisotropic Friedel oscillations are plotted from Eq. (14) for positive E_F. For negative E_F, the plot should be rotated by 90°.

II. FRIEDEL OSCILLATIONS

For a parabolic spectrum, $E_{\mathbf{k}} = \frac{\hbar^2 k^2}{2m}$, the Friedel oscillations of the electron density, $\delta n(\mathbf{r})$, created by a defect, are isotropic,

$$\delta n(\mathbf{r}) \propto \frac{\sin(2k_F r)}{(k_F r)^2}, \tag{2}$$

where $k_F = (\frac{2mE_F}{\hbar^2})^{1/2}$ is the Fermi wave vector.

Below we generalize the derivation of $\delta n(\mathbf{r})$ to the case of a hyperbolic spectrum Eq. (1) and demonstrate that it assumes the form

$$\delta n(\mathbf{r}) \propto \frac{\sin(2k_F\sqrt{x^2 - y^2})}{(k_F\sqrt{x^2 - y^2})^2}. \tag{3}$$

Outside the quadrants $|x| > |y|$, the correction $\delta\rho(\mathbf{r})$ falls off exponentially at large $r \gg k_F^{-1}$.

On the opposite side of the transition, $E_F < 0$, the result Eq. (3) transforms into

$$\delta n(\mathbf{r}) \propto \frac{\sin(2k_F\sqrt{y^2 - x^2})}{(k_F\sqrt{y^2 - x^2})^2}, \tag{4}$$

with $k_F = (\frac{2m|E_F|}{\hbar^2})^{1/2}$. Therefore, the crossing from positive to negative E_F is accompanied by rotation of the Friedel oscillations pattern by 90° (see Fig. 3). At finite temperature, T, the oscillations are cut off at distance r_T such that $k_F r_T \sim \frac{E_F}{T}$, so in the transition region $E_F \sim T$ the oscillations effectively disappear.

Derivation

Consider a short-range impurity with potential $U(\mathbf{r})$. It creates the following correction to the free-electron wave functions, $\Psi_{\mathbf{k}}(\mathbf{r})$:

$$\delta\Psi_{\mathbf{k}}(\mathbf{r}) = \sum_{\mathbf{k}'} \frac{U_{\mathbf{k}\mathbf{k}'}}{E_{\mathbf{k}} - E_{\mathbf{k}'}} \Psi_{\mathbf{k}'}(\mathbf{r}). \tag{5}$$

Then the electron density,

$$n(\mathbf{r}) = \sum_{\mathbf{k}} |\Psi_{\mathbf{k}}(\mathbf{r}) + \delta\Psi_{\mathbf{k}}(\mathbf{r})|^2 \Theta(E_F - E_{\mathbf{k}}), \tag{6}$$

acquires the following correction:

$$\delta n(\mathbf{r}) = 2\sum_{\mathbf{k}} \Theta(E_F - E_{\mathbf{k}}) \Psi^*_{\mathbf{k}} \delta\Psi_{\mathbf{k}}$$

$$= 2U_0 \sum_{\mathbf{k},\mathbf{k}'} \Theta(E_F - E_{\mathbf{k}}) \frac{\Psi^*_{\mathbf{k}}\Psi_{\mathbf{k}'}}{E_{\mathbf{k}} - E_{\mathbf{k}'}}, \tag{7}$$

where $U_0 = U_{\mathbf{k}\mathbf{k}'} = \int d\mathbf{r} U(\mathbf{r})$, and $\Theta(z)$ is a step function. It is convenient to rewrite Eq. (7) in the form

$$\delta n(\mathbf{r}) = \frac{U_0}{4\pi^2} \int_{-\infty}^{E_F} dE_1 \int_{-\infty}^{\infty} dE_2 \frac{\Phi(E_1, \mathbf{r})\Phi^*(E_2, \mathbf{r})}{E_1 - E_2}, \tag{8}$$

where we have introduced an auxiliary function

$$\Phi(E, \mathbf{r}) = \int d\mathbf{k} e^{i\mathbf{k}\mathbf{r}} \delta(E - E_{\mathbf{k}})$$

$$= \iint dk_x dk_y \delta\left[E - \frac{\hbar^2}{2m}\left(k_x^2 - k_y^2\right)\right] e^{ik_x x + ik_y y}. \tag{9}$$

To establish the analytical form of $\Phi(E, \mathbf{r})$, we switch to the new variables

$$k_x = p_x \cos\varphi_{\mathbf{r}} + p_y \sin\varphi_{\mathbf{r}},$$
$$k_y = p_x \sin\varphi_{\mathbf{r}} - p_y \cos\varphi_{\mathbf{r}}, \tag{10}$$

where $\varphi_{\mathbf{r}}$ is the azimuthal angle of $\mathbf{r}$. Then Eq. (9) takes the form

$$\Phi(E, \mathbf{r}) = \iint dp_x dp_y \delta\left[\frac{2mE}{\hbar^2} - \left(p_x^2 - p_y^2\right)\cos 2\varphi_{\mathbf{r}} - 2p_x p_y \sin 2\varphi_{\mathbf{r}}\right] e^{ip_x r}. \tag{11}$$

Note that p_y is present only in the argument of the δ function. To perform the integration over p_y, we factorize this argument:

$$\Phi(E, \mathbf{r}) = \frac{1}{\cos 2\varphi_{\mathbf{r}}} \int dp_x e^{ip_x r} \int dp_y \delta\left[\left(p_y + p_x \frac{\sin 2\varphi_{\mathbf{r}}}{\cos 2\varphi_{\mathbf{r}}} + \sqrt{\frac{p_x^2}{\cos^2 2\varphi_{\mathbf{r}}} - \left(\frac{2mE}{\hbar^2}\right)\frac{1}{\cos 2\varphi_{\mathbf{r}}}}\right)\right.$$
$$\left. \times \left(p_y + p_x \frac{\sin 2\varphi_{\mathbf{r}}}{\cos 2\varphi_{\mathbf{r}}} - \sqrt{\frac{p_x^2}{\cos^2 2\varphi_{\mathbf{r}}} - \left(\frac{2mE}{\hbar^2}\right)\frac{1}{\cos 2\varphi_{\mathbf{r}}}}\right)\right]. \tag{12}$$

Now the integration over p_y is straightforward and yields

$$\Phi(E, \mathbf{r}) = \frac{1}{2} \int_{-\infty}^{\infty} dp_x \frac{e^{ip_x r}}{\sqrt{p_x^2 - \left(\frac{2mE}{\hbar^2}\right)\cos 2\varphi_{\mathbf{r}}}}. \tag{13}$$

Here we assumed that $E\cos 2\varphi_{\mathbf{r}}$ is negative, so the expression under the square root does not turn to zero. Then the integral reduces to the Macdonald function. For positive $E\cos 2\varphi_{\mathbf{r}}$, the argument of the δ function in Eq. (12) turns to zero only when $|p_x| > [\frac{2mE}{\hbar^2 \cos 2\varphi_{\mathbf{r}}}]^{1/2}$. This condition excludes the interval $|p_x| < [\frac{2mE}{\hbar^2 \cos 2\varphi_{\mathbf{r}}}]^{1/2}$ from the integration. The integral then reduces to the Bessel function of the second kind. Combining both cases, we write

$$\Phi(E, \mathbf{r}) = \frac{m}{2\pi^2\hbar^2} \begin{cases} -Y_0(k_E\sqrt{x^2 - y^2}), & E(x^2 - y^2) > 0 \\ K_0(k_E\sqrt{y^2 - x^2}), & E(x^2 - y^2) < 0, \end{cases}$$

where $k_E = (\frac{2mE}{\hbar^2})^{1/2}$. In the case of a parabolic spectrum, the function $\Phi(E, \mathbf{r})$ is simply the Bessel function $J_0(k_E r)$.

Now the expression for $\Phi(E, \mathbf{r})$ should be substituted into Eq. (8). Similar to the parabolic spectrum, one has to use the large-argument asymptote of $\Phi(E, \mathbf{r})$. We see that for $|y| > |x|$, the Macdonald function decays exponentially, so there are no oscillations in two quadrants $|y| > |x|$. For quadrants $|x| > |y|$, the long-distance asymptote of $Y_0(z)$ is $\sin(z - \frac{\pi}{4})$, and differs by a phase $\pi/2$ from the asymptote, $\cos(z - \frac{\pi}{4})$, of $J_0(z)$. Thus, the product $Y_0(z_1)Y_0(z_2)$ contains $\cos(z_1 + z_2 - \frac{\pi}{2})$ in the same way as the product $J_0(z_1)J_0(z_2)$ only with *opposite sign*. This allows us to proceed directly to the result for $\delta n(\mathbf{r})$

$$\delta n(\mathbf{r}) = \frac{mU_0 \sin(2k_F\sqrt{x^2 - y^2})}{2\pi^2\hbar^2(x^2 - y^2)}. \tag{14}$$

Equation (14) illustrates the general connection [26] between the Friedel oscillations and the underlying spectrum. We note that the condition of applicability of the result Eq. (14) is that the argument of the sine is big.

III. SPECTRUM RENORMALIZATION

We start from the textbook expression [27] for the exchange self-energy,

$$\Sigma(\mathbf{k}) = -\int \frac{d^2k'}{(2\pi)^2} V(\mathbf{k} - \mathbf{k}')\, n_{\mathbf{k}'}, \tag{15}$$

where $n_{\mathbf{k}'} = \Theta(E_F - E_{\mathbf{k}'})$ is the Fermi distribution and $V(\mathbf{q})$ is the Fourier component of the electron-electron interaction. We first assume that $E_F = 0$ and choose for $V(\mathbf{q})$ the screened Coulomb potential,

$$V(\mathbf{q}) = \frac{2\pi e^2}{\epsilon(q + \kappa)}, \tag{16}$$

where ϵ is a bare dielectric constant and κ is the inverse screening radius which we will determine later.

Obviously, the integral over k' diverges at large k', leading to a general energy shift independent of k. To calculate the

spectrum renormalization, we subtract this shift and get

$$\Sigma(\mathbf{k})-\Sigma(0)=-\frac{2\pi e^2}{\epsilon}\int\frac{d^2k'}{(2\pi)^2}\frac{k'-|\mathbf{k}'-\mathbf{k}|}{(k'+\kappa)(|\mathbf{k}-\mathbf{k}'|+\kappa)}n_{\mathbf{k}'}. \tag{17}$$

Now the integral Eq. (17) converges at $k'\sim\kappa$. We are interested in the spectrum renormalization in the vicinity of the transition. Assuming that $k\ll\kappa$, we expand the integrand in parameter $\frac{k}{k'}$. This yields

$$\Sigma(\mathbf{k})-\Sigma(0) =-\frac{2\pi e^2}{\epsilon}\int\frac{d^2k'}{(2\pi)^2}\left[\frac{\frac{\mathbf{k}\cdot\mathbf{k}'}{k'}+\frac{(\mathbf{k}\cdot\mathbf{k}')^2-k^2k'^2}{2k'^3}}{(k'+\kappa)^2}+\frac{\left(\frac{\mathbf{k}\cdot\mathbf{k}'}{k'}\right)^2}{(k'+\kappa)^3}\right]n_{\mathbf{k}'}. \tag{18}$$

The expansion in Eq. (18) is carried out to the second order in $\frac{k}{k'}$, since the first-order term vanishes upon the angular integration. Indeed, this term changes sign upon replacement $\varphi_{\mathbf{k}'}\to(\pi-\varphi_{\mathbf{k}'})$, where $\varphi_{\mathbf{k}'}$ is the polar angle of the vector $\mathbf{k}'$. On the other hand, the argument of $n_{\mathbf{k}'}$ contains $\cos 2\varphi_{\mathbf{k}'}$, and it does not change upon this replacement. Thus, the integration of the linear term over $\varphi_{\mathbf{k}'}$ yields zero. The second and the third terms in Eq. (18) give rise to the following k^2 correction to the spectrum:

$$\Sigma(\mathbf{k})-\Sigma(0)=\frac{2\pi e^2}{\epsilon}k^2\int\frac{d^2k'}{(2\pi)^2} \times\left[\frac{\sin^2(\varphi_{\mathbf{k}}-\varphi_{\mathbf{k}'})}{2k'(k'+\kappa)^2}-\frac{\cos^2(\varphi_{\mathbf{k}}-\varphi_{\mathbf{k}'})}{(k'+\kappa)^3}\right]n_{\mathbf{k}'}. \tag{19}$$

It is instructive to rewrite this correction in the form

$$\Sigma(\mathbf{k})-\Sigma(0)=-\frac{2\pi e^2k^2}{\epsilon}\int\frac{d^2k'}{(2\pi)^2} \times\left[\frac{(k'-\kappa)+(3k'+\kappa)\cos 2(\varphi_{\mathbf{k}}-\varphi_{\mathbf{k}'})}{4k'(k'+\kappa)^3}\right]n_{\mathbf{k}'}. \tag{20}$$

We expect that interactions preserve the structure of the spectrum, $k^2\cos 2\varphi_{\mathbf{k}}$. On the other hand, the first term in the numerator of Eq. (20) leads to the isotropic k^2-correction. But it is easy to check that the condition

$$\int_0^\infty dk'\frac{k'-\kappa}{(k'+\kappa)^3}=0 \tag{21}$$

is met, so the coefficient in front of the k^2-term is zero. The final result for the spectrum renormalization reads

$$\Sigma(\mathbf{k})-\Sigma(0)=-k^2\cos 2\varphi_{\mathbf{k}}\left(\frac{e^2}{8\pi\epsilon}\right)\int_0^\infty\frac{dk'(3k'+\kappa)}{(k'+\kappa)^3} \times\int_0^{2\pi}d\varphi_{\mathbf{k}'}n_{\mathbf{k}'}\cos 2\varphi_{\mathbf{k}'}. \tag{22}$$

In Eq. (22), it is assumed that the Fermi level is zero. Then the integrals over k' and over $\varphi_{\mathbf{k}'}$ get decoupled. The first integral is equal to $2\kappa^{-1}$, while the second integral is equal to -2. It is convenient to cast Eq. (22) into the form of the renormalized mass in the spectrum Eq. (1):

$$\frac{1}{m_{\text{eff}}}=\frac{1}{m}\left(1+\frac{2me^2}{\pi\epsilon\kappa\hbar^2}\right). \tag{23}$$

At finite but small $E_F\ll\frac{\hbar^2\kappa^2}{2m}$, the dependence on E_F comes from the Fermi distribution $n_{\mathbf{k}'}=\Theta(E_F-\frac{\hbar^2}{k'^2}2m\cos 2\varphi_{\mathbf{k}'})$. At $E_F=0$, the argument of the Θ-function is positive when $\cos 2\varphi_{\mathbf{k}'}$ is negative. At finite E_F, the angular interval narrows, but slightly. This is because the typical value of k' is of the order of κ. On the other hand, the leading dependence on E_F originates from the parameter κ. Within the random-phase approximation, the expression for the inverse screening radius reads

$$\kappa=\frac{2\pi e^2}{\epsilon}\nu, \tag{24}$$

where ν is the density of states at the Fermi level. In fact, ν diverges in the limit $E_F\to 0$. Indeed, one has

$$\nu(E)=2\int\frac{d^2k}{(2\pi)^2}\delta\left[E-\frac{\hbar^2}{2m}\left(k_x^2-k_y^2\right)\right]=\frac{2m}{\pi^2\hbar^2}\ln\left(\frac{\tilde{E}_F}{|E|}\right). \tag{25}$$

Substituting Eq. (25) into Eq. (24), we arrive at the following expression for renormalized mass:

$$\frac{1}{m_{\text{eff}}}=\frac{1}{m}\left[1+\frac{1}{2\ln(\tilde{E}_F/|E_F|)}\right]. \tag{26}$$

IV. POLARIZATION OPERATOR

The polarization operator for 2D electron gas with a parabolic spectrum was calculated by F. Stern [28]. Below we calculate the polarization operator for a hyperbolic spectrum Eq. (1), we start from the definition

$$\Pi(\omega,\boldsymbol{q})=\sum_{\mathbf{k}}\frac{n_{\mathbf{k}}-n_{\mathbf{k}+\mathbf{q}}}{\hbar\omega+E_{\mathbf{k}}-E_{\mathbf{k}+\mathbf{q}}}. \tag{27}$$

As a first step, we cast Eq. (27) into the form

$$\Pi(\omega,\boldsymbol{q})=\sum_{\mathbf{k}}n_{\mathbf{k}}\left[\frac{1}{\hbar\omega+E_{\mathbf{k}}-E_{\mathbf{k}+\mathbf{q}}}-\frac{1}{\hbar\omega+E_{\mathbf{k}-\mathbf{q}}-E_{\mathbf{k}}}\right]. \tag{28}$$

Introducing, similar to Eqs. (10), the new variables

$$k_x=p_x\cos\varphi_{\mathbf{q}}+p_y\sin\varphi_{\mathbf{q}},\qquad k_y=p_y\cos\varphi_{\mathbf{q}}-p_x\sin\varphi_{\mathbf{q}}, \tag{29}$$

and replacing the sum by the integral, we obtain

$$\Pi(\omega,\boldsymbol{q})=\iint\frac{dp_xdp_y}{(2\pi)^2}\Theta\left[\frac{2mE_F}{\hbar^2}-\left(p_x^2-p_y^2\right)\times\cos 2\varphi_{\mathbf{q}}-2p_xp_y\sin 2\varphi_{\mathbf{q}}\right] \times\left[\frac{1}{\hbar\omega+\frac{\hbar^2q^2}{2m}\cos 2\varphi_{\mathbf{q}}-\frac{\hbar^2}{m}p_xq}-\frac{1}{\hbar\omega-\frac{\hbar^2q^2}{2m}\cos 2\varphi_{\mathbf{q}}-\frac{\hbar^2}{m}p_xq}\right]. \tag{30}$$

Note that the argument of the Θ function has the same form as the argument of the δ function in Eq. (12) with $\varphi_{\mathbf{q}}$ instead of $\varphi_{\mathbf{r}}$. Then the integration over p_y is straightforward,

$$\Pi(\omega,\boldsymbol{q}) = \int_{-\infty}^{\infty} \frac{dp_x}{2\pi^2}\left[\frac{p_x^2}{\cos^2 2\varphi_{\mathbf{q}}} - \frac{2mE_F}{\hbar^2\cos 2\varphi_{\mathbf{q}}}\right]^{1/2} \times\left[\frac{\hbar\omega + \frac{\hbar^2q^2}{2m}\cos 2\varphi_{\mathbf{q}}}{\left(\hbar\omega + \frac{\hbar^2q^2}{2m}\cos 2\varphi_{\mathbf{q}}\right)^2 - \left(\frac{\hbar^2 p_x q}{m}\right)^2} - \frac{\hbar\omega - \frac{\hbar^2q^2}{2m}\cos 2\varphi_{\mathbf{q}}}{\left(\hbar\omega - \frac{\hbar^2q^2}{2m}\cos 2\varphi_{\mathbf{q}}\right)^2 - \left(\frac{\hbar^2 p_x q}{m}\right)^2}\right], \quad (31)$$

where the first square bracket is the result of integration over p_y, and in the second square bracket we have isolated the parts even in p_x.

It is convenient to rewrite Eq. (31) as follows:

$$\Pi(\omega,\boldsymbol{q}) = \frac{m}{\pi^2\hbar^2 q\cos 2\varphi_{\mathbf{q}}}\int dp_x\left[p_x^2 - A\right]^{1/2} \times\left[\frac{\beta_+}{\beta_+^2 - p_x^2} - \frac{\beta_-}{\beta_-^2 - p_x^2}\right], \quad (32)$$

where the parameters A, β_+, and β_- are defined as

$$A = \frac{2mE_F\cos 2\varphi_{\mathbf{q}}}{\hbar^2},$$
$$\beta_\pm = \frac{m}{\hbar^2 q}\left(\hbar\omega \pm \frac{\hbar^2q^2}{2m}\cos 2\varphi_{\mathbf{q}}\right). \quad (33)$$

Now the integration in Eq. (32) can be performed explicitly. The main contribution to the polarization operator comes from log divergence of the integral at large p_x. This divergence is cut off at $p_x \sim (2m\tilde{E}_F/\hbar^2)^{1/2}$. The ω and q dependencies are given by the subleading terms

$$\Pi(\omega,\boldsymbol{q}) = \frac{m}{\pi^2\hbar^2 q\cos 2\varphi_{\mathbf{q}}} \times\left[-(\beta_+ - \beta_-)\ln\left(\frac{\tilde{E}_F}{|E_F\cos 2\varphi_{\mathbf{q}}|}\right) - \left(\frac{\beta_+^2 - A}{\beta_+}\right)G\left(\frac{A}{\beta_+^2}\right) + \left(\frac{\beta_-^2 - A}{\beta_-}\right)G\left(\frac{A}{\beta_-^2}\right)\right], \quad (34)$$

where the function $G(z)$ is defined as

$$G(z) = \int \frac{d\mathcal{P}}{(\mathcal{P}^2 - z)^{1/2}(\mathcal{P}^2 - 1)}. \quad (35)$$

The upper limit in the integral Eq. (35) is infinity. The lower limit is $p_y = z^{1/2}$ for positive z and $p_y = 0$ for negative z. Correspondingly, the form of $G(z)$ is different for $z > 0$ and $z < 0$. Namely,

$$G(z) = \begin{cases} \frac{1}{(z-1)^{1/2}}\arcsin\left(\frac{1}{z^{1/2}}\right), & z > 0 \\ \frac{\ln\left(\frac{1}{|z|^{1/2}} + \sqrt{1+\frac{1}{|z|}}\right)}{(|z|+1)^{1/2}}, & z < 0, \end{cases}$$

It is easy to see that $G(z)$ falls off as $1/z$ at large positive z and as $1/|z|$ at large negative z.

A. Frequency domain

Note that the coefficient $(\beta_+ - \beta_-)$ in front of the leading logarithmic term does not depend on frequency. In 2D electron gas with parabolic spectrum [28], the analog of the combinations $\beta_\pm^2 - A$ in Eq. (34) has the form $[(\hbar\omega - \frac{\hbar^2q^2}{2m})^2 - 2\frac{\hbar^2q^2\tilde{E}_F}{m}]^{1/2}$. At small q, the polarization operator acquires an imaginary part, which is responsible for the AC conductivity, when $\omega > (\frac{2\tilde{E}_F}{m})^{1/2}q$. The corresponding condition for the hyperbolic spectrum reads $\omega > (\frac{2E_F\cos 2\varphi_{\mathbf{q}}}{m})^{1/2}q$. First, since $\tilde{E}_F$, the Fermi energy in the "bulk" is much bigger than E_F, we conclude that the AC response at low frequencies is dominated by the proximity to the topological transition. Second, this response is strongly anisotropic.

B. Momentum domain

In the static limit, $\omega = 0$, the polarization operator is a universal function of the dimensionless momentum:

$$Q_{\mathbf{q}} = q\left(\frac{\hbar^2}{2mE_F}\cos 2\varphi_{\mathbf{q}}\right)^{1/2}. \quad (36)$$

This function has a form

$$\Pi(\mathbf{q}) = -\frac{m}{2\pi^2\hbar^2}\left[\ln\left(\frac{\tilde{E}_F}{|E_F\cos 2\varphi_{\mathbf{q}}|}\right) - \left(1 - \frac{Q_{\mathbf{q}}^2}{4}\right)^{1/2}\frac{\arcsin\left(\frac{Q_{\mathbf{q}}}{2}\right)}{\left(\frac{Q_{\mathbf{q}}}{2}\right)}\right] \quad (37)$$

for $|Q_{\mathbf{q}}| < 2$. Near the Kohn anomaly, the behavior of $(\Pi(\mathbf{q}) - \Pi(0))$ is singular, $(2 - |Q_{\mathbf{q}}|)^{1/2}$. It gives rise to the long-period Friedel oscillations Eq. (14).

For $|Q_{\mathbf{q}}| > 2$, the expression for the polarization operator reads

$$\Pi(\mathbf{q}) = -\frac{m}{2\pi^2\hbar^2}\left\{\ln\left(\frac{\tilde{E}}{|E_F\cos 2\varphi_{\mathbf{q}}|}\right) + \left(1 - \frac{4}{Q_{\mathbf{q}}^2}\right)^{1/2} \times\ln\left[\left(\frac{Q_{\mathbf{q}}}{2}\right) + \sqrt{\frac{Q_{\mathbf{q}}^2}{4} - 1}\right]\right\}. \quad (38)$$

As a function of $(|Q_{\mathbf{q}}| - 2)$, the behavior of $\Pi(\mathbf{q})$ is linear. Note that the behaviors Eqs. (37) and (38) differ from the static polarization operator for the isotropic spectrum [28], where $\Pi(\mathbf{q})$ is constant for $q < 2k_F$, while the Kohn anomaly, $\propto(q - 2k_F)^{1/2}$, is located to the right from $q = 2k_F$.

To summarize, we have evaluated a polarization operator in the entire domain of frequencies and momenta. In the static limit and for $q_y = 0$, our result agrees with Ref. [22]. While for parabolic spectrum, $E_{\mathbf{k}} = \frac{\hbar^2}{2m}(k_x^2 + k_y^2)$, the Kohn anomaly corresponds to the condition $q = 2k_F$, the corresponding condition for the hyperbolic spectrum Eq. (1) reads

$$q_x^2 - q_y^2 = 4k_F^2. \quad (39)$$

This condition is illustrated in Fig. 2.

V. ELECTRON LIFETIME

The process which is responsible for a finite lifetime, τ_e, of an electron with energy, $E_{\mathbf{k}}$, above the Fermi level is the creation of an electron-hole pair. Accurate calculation of τ_e for an electron gas with a parabolic spectrum was reported in Refs. [29,30]. The result reads

$$\frac{1}{\tau_{\mathbf{k}}} = \Gamma(\mathbf{k}, E_{\mathbf{k}}) = \frac{E_{\mathbf{k}}^2}{4\pi\hbar\tilde{E}_F} \ln\left(\frac{\tilde{E}_F}{E_{\mathbf{k}}}\right). \tag{40}$$

The $E_{\mathbf{k}}^2$ dependence originates from the energy conservation, namely $E_{\mathbf{k}} + E_{\mathbf{p}} = E_{\mathbf{k}'} + E_{\mathbf{p}'}$, where $E_{\mathbf{k}'} > \tilde{E}_F$ is the energy of the secondary electron, while $E_{\mathbf{p}} < \tilde{E}_F$ and $E_{\mathbf{p}'} > \tilde{E}_F$ are the energies of particles constituting an excited pair. The factor $\ln\left(\frac{\tilde{E}_F}{E_{\mathbf{k}}}\right)$ originates from the momentum conservation. To generalize Eq. (40) to the case of hyperbolic spectrum, we start from the golden-rule expression for the rate $\tau_{\mathbf{k}}^{-1}$:

$$\frac{1}{\tau_{\mathbf{k}}} \propto \int_{E_{\mathbf{k}'}>\tilde{E}_F} d\mathbf{k}' \int_{E_{\mathbf{p}}<\tilde{E}_F} d\mathbf{p} \int_{E_{\mathbf{p}'}>\tilde{E}_F} d\mathbf{p}' \times \delta(E_{\mathbf{k}} + E_{\mathbf{p}} - E_{\mathbf{k}'} - E_{\mathbf{p}'})\delta(\mathbf{k} + \mathbf{p} - \mathbf{k}' - \mathbf{p}'). \tag{41}$$

In conventional calculations [29,30], the interaction strength is absent in Eq. (41) as a result of screening. In our case, the screening radius, κ^{-1}, contains an additional logarithmic factor, which we do not capture in our calculations.

To perform the averaging over the directions of momenta, we introduce auxiliary variables E_1, E_2, and E_3 and invoke the integral representation of the δ function:

$$\frac{1}{\tau_{\mathbf{k}}} \propto \int_{\tilde{E}_F}^{\infty} dE_1 \int_{-\infty}^{\tilde{E}_F} dE_2 \int_{\tilde{E}_F}^{\infty} dE_3\, \delta(E_{\mathbf{k}} + E_2 - E_1 - E_3) \times \int d\mathbf{k}' \int d\mathbf{p} \int d\mathbf{p}' \delta(E_{\mathbf{k}'} - E_1)\delta(E_{\mathbf{p}} - E_2)\delta(E_{\mathbf{p}'} - E_3) \times \int \frac{d\mathbf{r}}{(2\pi)^2} \exp[i(\mathbf{k} + \mathbf{p} - \mathbf{k}' - \mathbf{p}')\mathbf{r}]. \tag{42}$$

Now the integration over momenta decouples into three integrals of the type $\int d\mathbf{p} \exp(i\mathbf{pr})\delta(E_{\mathbf{p}} - E)$. For a parabolic spectrum, this integral is expressed through a zero-order Bessel function, $J_0(k_E r)$. Then the integral over $\mathbf{r}$ in Eq. (42) assumes the form

$$I = \int d\mathbf{r} e^{i\mathbf{kr}} J_0(k_{E_1} r) J_0(k_{E_2} r) J_0(k_{E_3} r). \tag{43}$$

The angular-averaged $\exp(i\mathbf{kr})$ is equal to $J_0(k_E r)$. The magnitudes of all momenta in Eq. (43) are close to the Fermi momentum, $\tilde{k}_F$. The long-distance behavior of the product of the four Bessel functions is $\propto \frac{1}{(\tilde{k}_F r)^2}$. Then the integration over r gives rise to the logarithm in Eq. (40), while $\frac{1}{\tilde{k}_F^2}$ generates $\tilde{E}_F$ in the denominator.

For a hyperbolic spectrum, the integral $\int d\mathbf{p} \exp(i\mathbf{pr})\delta(E_{\mathbf{p}} - E)$ is given by the function $\Phi(E, \mathbf{r})$ defined by Eq. (9). Then, in place of integral Eq. (43), one has

$$I = \int d\mathbf{r} e^{i\mathbf{kr}} \Phi(E_1, \mathbf{r})\Phi(E_2, \mathbf{r})\Phi(E_3, \mathbf{r}). \tag{44}$$

Depending on the polar angle of $\mathbf{r}$, the function $\Phi(E, \mathbf{r})$ either oscillates with r (in the domain $-\frac{\pi}{4} < \varphi_{\mathbf{r}} < \frac{\pi}{4}$) or decays with r (in the domain $\frac{\pi}{4} < \varphi_{\mathbf{r}} < \frac{3\pi}{4}$). In the first domain, with energies E_1, E_2, E_3 close to E_F and wave vector k close to $(2mE_F/\hbar^2)^{1/2}$, the slow part of the integrand in Eq. (44) reproduces, within a numerical factor, the result Eq. (40) for the hyperbolic spectrum.

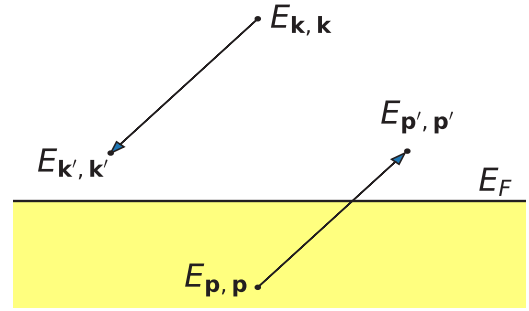

FIG. 4. Illustration of the process responsible for a finite electron lifetime: Initial electron with momentum $\mathbf{k}$ and energy E_k reduces its energy and goes to the final state $E_{\mathbf{k}'}$, creating a pair with energies $E_{\mathbf{p}}$ and $E_{\mathbf{p}'}$.

Naturally, the applicability of Eq. (40) requires that $|E_{\mathbf{k}} - E_F| \ll E_F$. In the vicinity of the topological transition, E_F is small and the estimate for the lifetime follows from Eq. (40) upon setting $E_F \sim E_{\mathbf{k}}$. We conclude that, in the vicinity of the topological transition, $\frac{\hbar}{\tau_e} \sim E$.

Assume now that the Fermi level is $E_F = 0$. The question of interest is how τ_e depends on the direction, $\varphi_{\mathbf{k}}$, of the momentum of the initial electron. For $E_F = 0$, energy conservation requires that, when the energy E_1 is positive, the energy E_2 is negative while the energy E_3 is positive, see Fig. 4. Then Eq. (44) assumes the form

$$I = \int_0^{\infty} dr r \int_0^{2\pi} d\varphi_{\mathbf{r}} \exp[ikr\cos(\varphi_{\mathbf{k}} - \varphi_{\mathbf{r}})] \times Y_0(k_1 r\cos 2\varphi_{\mathbf{r}}) K_0(k_2 r\cos 2\varphi_{\mathbf{r}}) Y_0(k_3 r\cos 2\varphi_{\mathbf{r}}), \tag{45}$$

where k is the magnitude of momentum of initial electron, k_1 and k_3 are momenta of the secondary electrons, and $-k_2$ is the momentum of a hole.

To find the dependence of τ_e on $\varphi_{\mathbf{k}}$, we introduce instead of r a new variable $z = kr\cos 2\varphi_{\mathbf{r}}$ and obtain

$$I = \frac{1}{k^2} \int_0^{2\pi} \frac{d\varphi_{\mathbf{r}}}{\cos^2 2\varphi_{\mathbf{r}}} \int_0^{\infty} dz z \exp\left[iz\frac{\cos(\varphi_{\mathbf{k}} - \varphi_{\mathbf{r}})}{\cos 2\varphi_{\mathbf{r}}}\right] \times Y_0\left(\frac{k_1}{k}z\right) K_0\left(\frac{k_2}{k}z\right) Y_0\left(\frac{k_3}{k}z\right). \tag{46}$$

The form Eq. (46) suggests that the main contribution to the integral comes from the vicinity of $\varphi_{\mathbf{r}} \approx \pm\frac{\pi}{4}, \pm\frac{3\pi}{4}$. For these $\varphi_{\mathbf{r}}$, the exponent in the integrand rapidly oscillates with z. The exceptions are the vicinities of $\varphi_{\mathbf{k}} = \pm\frac{\pi}{4}, \pm\frac{3\pi}{4}$ when $\cos(\varphi_{\mathbf{k}} - \varphi_{\mathbf{r}})$ turns to zero when $\varphi_{\mathbf{r}}$ is close to $\pm\frac{\pi}{4}, \pm\frac{3\pi}{4}$.

As an example, consider a situation $\varphi_{\mathbf{k}} \approx -\frac{\pi}{4}$ and set $\varphi_{\mathbf{r}} = \frac{\pi}{4} + \psi_{\mathbf{r}}$, with $\psi_{\mathbf{r}} \ll 1$. The exponent in Eq. (46) does not

oscillate for $\psi_{\mathbf{r}} > \psi_{\min}$, where $\psi_{\min} = |\cos(\varphi_{\mathbf{k}} - \frac{\pi}{4})|$. Then the angular integration in Eq. (46) yields

$$\int_{\psi_{\min}}^{\infty} \frac{d\psi_{\mathbf{r}}}{\psi_{\mathbf{r}}^2} = \frac{1}{\psi_{\min}} = \frac{1}{|\cos(\varphi_{\mathbf{k}} - \frac{\pi}{4})|}. \tag{47}$$

The above result suggests that the lifetime, τ_e, shortens dramatically for certain directions of momentum of an electron. Physical explanation of such a shortening is that the cost of creation of a pair by electron with these directions of momentum is anomalously low.

VI. CONCLUDING REMARKS

(i) Ballistic correction to the conductivity [31–33], $\sigma(E_F, T)$, of a 2D electron gas has the form $\frac{\delta\sigma}{\sigma} \sim \lambda(\frac{T}{E_F})$, where λ is the interaction parameter [32]. The origin of this correction is electron scattering from the potential created by Friedel oscillations surrounding individual impurities. The amplitude of this process is sharply peaked at the scattering angle π. For this angle, the momentum transfer is close to $2k_F$, the wave vector of the Friedel oscillation. For the hyperbolic spectrum, while the wave vector of the Friedel oscillations depends on the direction, the mechanism of Refs. [31,32] still applies. It gets modified as illustrated in Fig. 2. Backscattering takes place between disjoint parts of the Fermi surface. The smallness of E_F makes the ballistic correction progressively pronounced in the vicinity of the transition.

(ii) While calculating the spectrum renormalization, we assumed that the form of interaction is screened Coulomb, see Eq. (16). In fact, the static polarization operator Eq. (37) contains a subleading term, $(1 - \frac{Q_{\mathbf{q}}^2}{4})^{1/2}$, describing the Kohn anomaly. This term is strongly anisotropic. An interesting question is how this anisotropy affects the spectrum renormalization. Denote with $\delta\kappa(\mathbf{q})$ the correction to the inverse screening radius, describing the Kohn anomaly, $\delta\kappa(\mathbf{q}) \propto (1 - \frac{\hbar^2 q^2}{8mE_F}\cos 2\varphi_{\mathbf{q}})^{1/2}$. Expanding the interaction $V(\mathbf{q})$ with respect to $\delta\kappa(\mathbf{q})$, we get

$$\delta V(\mathbf{q}) = -\frac{2\pi e^2 \delta\kappa(\mathbf{q})}{\epsilon(q+\kappa)^2}. \tag{48}$$

This correction to $V(\mathbf{q})$ gives rise to the following correction to the self-energy:

$$\delta\Sigma(\mathbf{k}) \propto \int d\mathbf{k}' \delta\kappa(\mathbf{k} - \mathbf{k}')\Theta\left(E_F - \frac{\hbar^2 k'^2}{2m}\cos 2\varphi_{\mathbf{k}'}\right). \tag{49}$$

At small momenta, $|k| \ll k_F$, Eq. (49) leads to the following contribution to the spectrum renormalization:

$$\delta\Sigma(\mathbf{k}) \propto E_{\mathbf{k}} \int d\mathbf{k}' \frac{E_{\mathbf{k}'}}{(E_F - E_{\mathbf{k}'})^{3/2}}\Theta(E_F - E_{\mathbf{k}'}). \tag{50}$$

This correction diverges; the divergence comes from the vicinity of $\varphi_{\mathbf{k}} = \pm\frac{\pi}{4}, \pm\frac{3\pi}{4}$.

(iii) The divergence of lifetime for directions of momenta close to $\varphi_{\mathbf{q}} = \pm\frac{\pi}{4}, \pm\frac{3\pi}{4}$ also hints at strong renormalization of the spectrum for these momenta.

(iv) With regard to observables, interaction-induced modification of the effective mass manifests itself in the magneto-oscillations. Behavior of magneto-oscillations in the vicinity of the topological transition constitutes a subfield called the magnetic breakdown, see, e.g., the review Ref. [34]. As the Fermi level is swept through the topological transition, the period of magneto-oscillations doubles. The width of the domain of E_F where this doubling takes place is $\sim\frac{\hbar^2}{ml^2}$, where l is the magnetic length. For $E_F \gg \frac{\hbar^2}{ml^2}$, the coupling of the semiclassical trajectories is determined by tunneling under the magnetic barrier [35]. Then the dependence of the effective mass on E_F affects the barrier transmission.

Electron lifetime is measured in 2D-2D tunneling experiments [36,37]. The lifetime defines the width of the peak in the tunnel conductance measured versus the DC bias applied between the layers.

With regard to materials, see, e.g., Refs. [38–42], with band structure governed by spin-orbit coupling, our main message is that when the Fermi level is located in the vicinity of the Van Hove singularity, like the nodal line [21], the Fermi-liquid description of the electron states fails due to the production of soft electron-hole pairs. This situation is realized in certain topological crystalline insulators [38–42]. Since most experimental studies of topological materials are carried out using spectroscopic measurements (ARPES) [43], we predict that, if the Fermi level can be tuned, the photoemission line becomes anomalously broad at the Lifshitz transition.

(v) There is a conceptual similarity between Friedel oscillations of elections of the electron density created by an impurity and the oscillations of the spin density created by a magnetic impurity [44]. In this regard, long-period Friedel oscillations in the vicinity of the topological transition are similar to the long-period behavior of the RKKY interaction established in Ref. [17].

ACKNOWLEDGMENT

The work was supported by the Department of Energy, Office of Basic Energy Sciences, Grant No. DE-FG02-06ER46313.

[1] I. M. Lifshitz, Anomalies of electron characteristics of a metal in the high pressure region, Sov. Phys. JETP **11**, 1130 (1960).

[2] V. S. Egorov and A. N. Fedorov, Thermopower of lithium-magnesium alloys at the 21/2 -order transition, Sov. Phys. JETP **58**, 959 (1983).

[3] N. V. Zavaritskii and I. M. Suslov, Structural features in the thermopower of a two-dimensional electron gas near topological transitions, Sov. Phys. JETP **60**, 1243 (1984).

[4] E. A. Yelland, J. M. Barraclough, W. Wang, K. V. Kamenev, and A. D. Huxley, High-field superconductivity at an electronic topological transition in URhGe, Nat. Phys. **7**, 890 (2011).

[5] M. Orlita, P. Neugebauer, C. Faugeras, A. L. Barra, M. Potemski, F. M. D. Pellegrino, and D. M. Basko, Cyclotron Motion in the Vicinity of a Lifshitz Transition in Graphite, Phys. Rev. Lett. **108**, 017602 (2012).

[6] A. Varleta, M. Mucha-Kruczyński, D. Bischoff, P. Simonet, T. Taniguchi, K. Watanabe, V. Fal'ko, T. Ihn, and K. Ensslin, Tunable Fermi surface topology and Lifshitz transition in bilayer graphene, Synth. Met. **210**, 19 (2015).

[7] H.-R. Chang, J. Zhou, H. Zhang, and Y. Yao, Probing the topological phase transition via density oscillations in silicene and germanene, Phys. Rev. B **89**, 201411(R) (2014).

[8] H. Chi, C. Zhang, G. Gu, D. E. Kharzeev, X. Dai, and Q. Li, Lifshitz transition mediated electronic transport anomaly in bulk $ZrTe_5$, New J. Phys. **19**, 015005 (2017).

[9] M. E. Barber, A. S. Gibbs, Y. Maeno, A. P. Mackenzie, and C. W. Hicks, Resistivity in the Vicinity of a Van Hove Singularity: Sr_2RuO_4 Under Uniaxial Pressure, Phys. Rev. Lett. **120**, 076602 (2018).

[10] P. Di Pietro, M. Mitrano, S. Caramazza, F. Capitani, S. Lupi, P. Postorino, F. Ripanti, B. Joseph, N. Ehlen, A. Grüneis, A. Sanna, G. Profeta, P. Dore, and A. Perucchi, Emergent Dirac carriers across a pressure-induced Lifshitz transition in black phosphorus, Phys. Rev. B **98**, 165111 (2018).

[11] T. Nishimura, H. Sakai, H. Mori, K. Akiba, H. Usui, M. Ochi, K. Kuroki, A. Miyake, M. Tokunaga, Y. Uwatoko, K. Katayama, H. Murakawa, and N. Hanasaki, Large Enhancement of Thermoelectric Efficiency Due to a Pressure-Induced Lifshitz Transition in SnSe, Phys. Rev. Lett. **122**, 226601 (2019).

[12] A. A. Varlamov and A. V. Pantsulaya, Anomalous kinetic properties of metals near the Lifshitz topological transition, Sov. Phys. JETP **62**, 1263 (1985).

[13] A. A. Varlamov and A. V. Pantsulaya, Absorption of iongitudinal sound in metals near the Lifshitz topological transition, Sov. Phys. JETP **64**, 1319 (1986).

[14] Y. M. Blanter, A. A. Varlamov, and A. V. Pantsulaya, Giant oscillations of the magnetothermoelectric power of a metal near an electronic topological transition, Sov. Phys. JETP **70**, 695 (1990).

[15] Y. M. Blanter, A. A. Varlamov, and A. V. Pantsulaya, Thermoelectric power and topological transitions in quasi-2D electron systems, Sov. Phys. JETP **73**, 688 (1991).

[16] N. N. Ablyazov, M. Yu. Kuchiev, and M. E. Raikh, Topological transition and its connection with the conductivity and thermopower anomalies in two-dimensional systems, Phys. Rev. B **44**, 8802 (1991).

[17] D. I. Golosov and M. I. Kaganov, Spatial correlation of conduction electrons near the electron-topological transition in a metal, Sov. Phys. JETP **74**, 186 (1992).

[18] M. I. Kaganov and A. Möbius, Effect of Fermi-liquid interaction on a phase transition of order 21/2, Sov. Phys. JETP **59**, 405 (1984).

[19] Y. M. Blanter, M. I. Kaganov, A. V. Pantsulaya, and A. A. Varlamov, The theory of electronic topological transitions, Phys. Rep. **245**, 159 (1994).

[20] K. Seo, C. Zhang, and S. Tewari, Thermodynamic signatures for topological phase transitions to Majorana and Weyl superfluids in ultracold Fermi gases, Phys. Rev. A **87**, 063618 (2013).

[21] J.-W. Rhim and Y. B. Kim, Anisotropic density fluctuations, plasmons, and Friedel oscillations in nodal line semimetal, New J. Phys. **18**, 043010 (2016).

[22] C.-K. Lu, Friedel oscillation near a van Hove singularity in two-dimensional Dirac materials, J. Phys.: Condens. Matter **28**, 065001 (2016).

[23] T. Farajollahpour, S. Khamouei, S. S. Shateri, and A. Phirouznia, Anisotropic Friedel oscillations in graphene-like materials: The Dirac point approximation in wave-number dependent quantities revisited, Sci. Rep. **8**, 2667 (2018).

[24] G. E. Volovik, Exotic Lifshitz transitions in topological materials, Phys. Usp. **61**, 89 (2018).

[25] Y. M. Galperin, D. Grassano, V. P. Gusynin, A. V. Kavokin, O. Pulci, S. G. Sharapov, V. O. Shubnyi, and A. A. Varlamov, Entropy signatures of topological phase transitions, J. Exp. Theor. Phys. **127**, 958 (2018).

[26] C. Bena, Friedel oscillations: Decoding the hidden physics, C. R. Phys. **17**, 302 (2016).

[27] G. Mahan, *Many-Particle Physics, Physics of Solids and Liquids* (Springer, New York, 2010).

[28] F. Stern, Polarizability of a Two-Dimensional Electron Gas, Phys. Rev. Lett. **18**, 546 (1967).

[29] T. Jungwirth and A. H. MacDonald, Electron-electron interactions and two-dimensional−two-dimensional tunneling, Phys. Rev. B **53**, 7403 (1996).

[30] L. Zheng and S. Das Sarma, Coulomb scattering lifetime of a two-dimensional electron gas, Phys. Rev. B **53**, 9964 (1996).

[31] A. Gold and V. T. Dolgopolov, Temperature dependence of the conductivity for the two-dimensional electron gas: Analytical results for low temperatures, Phys. Rev. B **33**, 1076 (1986).

[32] G. Zala, B. N. Narozhny, and I. L. Aleiner, Interaction corrections at intermediate temperatures: Longitudinal conductivity and kinetic equation, Phys. Rev. B **64**, 214204 (2001).

[33] Y. Adamov, I. V. Gornyi, and A. D. Mirlin, Interaction effects on magneto-oscillations in a two-dimensional electron gas, Phys. Rev. B **73**, 045426 (2006).

[34] M. I. Kaganov and A. A. Slutskin, Coherent magnetic breakdown, Phys. Rep. **98**, 189 (1983).

[35] G. E. Zil'berman, Electron in a periodic electric and homogeneous magnetic field, II, Sov. Phys. JETP **6**, 299 (1958).

[36] J. P. Eisenstein, T. J. Gramila, L. N. Pfeiffer, and K. W. West, Probing a two-dimensional Fermi surface by tunneling, Phys. Rev. B **44**, 6511 (1991).

[37] S. Q. Murphy, J. P. Eisenstein, L. N. Pfeiffer, and K. W. West, Lifetime of two-dimensional electrons measured by tunneling spectroscopy, Phys. Rev. B **52**, 14825 (1995).

[38] T. H. Hsieh, H. Lin, J. Liu, W. Duan, A. Bansil, and L. Fu, Topological crystalline insulators in the SnTe material class, Nat. Commun. **3**, 982 (2012).

[39] A. S. Rodin, A. Carvalho, and A. H. Castro Neto, Strain-Induced Gap Modification in Black Phosphorus, Phys. Rev. Lett. **112**, 176801 (2014).

[40] A. Ziletti, S. M. Huang, D. F. Coker, and H. Lin, Van Hove singularity and ferromagnetic instability in phosphorene, Phys. Rev. B **92**, 085423 (2015).

[41] N. P. Armitage, E. J. Mele, and A. Vishwanath, Weyl and Dirac semimetals in three-dimensional solids, Rev. Mod. Phys. **90**, 015001 (2018).

[42] H. F. Yang, L. X. Yang, Z. K. Liu, Y. Sun, C. Chen, H. Peng, M. Schmidt, D. Prabhakaran, B. A. Bernevig, C. Felser, B. H.

Yan, and Y. L. Chen, Topological Lifshitz transitions and Fermi arc manipulation in Weyl semimetal NbAs, Nat. Commun. **10**, 3478 (2019).

[43] L. Huang, T. M. McCormick, M. Ochi, Z. Zhao, M. Suzuki, R. Arita, Y. Wu, D. Mou, H. Cao, J. Yan, N. Trivedi, and A. Kaminski, Spectroscopic evidence for type II Weyl semimetal state in $MoTe_2$, Nat. Mater. **15**, 1155 (2016).

[44] L. M. Roth, H. J. Zeiger, and T. A. Kaplan, Generalization of the Ruderman-Kittel-Kasuya-Yosida interaction for nonspherical Fermi surfaces, Phys. Rev. **149**, 519 (1966).